Pulay forces from localized orbitals optimized *in situ* using a psinc basis set

Álvaro Ruiz-Serrano,[1] Nicholas D. M. Hine,[2] and Chris-Kriton Skylaris[1, a)]

[1)] *School of Chemistry, University of Southampton, Highfield, Southampton SO17 1BJ, UK.*

[2)] *Department of Physics and Department of Materials, Imperial College London, Exhibition Road, London SW7 2AZ, UK.*

(Dated: 16 April 2012)

In-situ optimization of a set of localized orbitals with respect to a systematically improvable psinc basis set independent of the position of the atoms would theoretically eliminate the Pulay contribution to the total ionic forces. In this work we show that for strict localization constraints, especially with small localization regions, there can be non-negligible Pulay forces that must be calculated. Geometry optimization calculations of molecular systems which heavily rely upon accurate evaluation of the ionic forces are much better behaved when the Pulay forces are included. The more conventional case where the local orbitals remain fixed to Pseudo-Atomic Orbital (PAO) multiple-zeta basis sets also benefits from this implementation. We have validated the method on several test cases, including a DNA fragment with 1045 atoms.

Keywords: Ionic forces, Geometry optimization, Pseudoatomic orbitals

[a)] Electronic mail: C.Skylaris@soton.ac.uk

I. INTRODUCTION

Quantum mechanical methods based on Kohn-Sham Density Functional Theory (DFT)[1,2] are widely used to determine properties of materials and molecules at the level of quantum theory. The computational cost of traditional approaches to DFT[3–7] scales as $\mathcal{O}(N^3)$, where N is the number of atoms in the system, usually limiting the range of calculations to no more than some hundreds of atoms. Increasing efforts have been put in the development of linear-scaling approaches based on the principle of *nearsightedness* of electronic matter[8], which establishes that the single-particle density matrix in systems with non-zero band gap decays exponentially with the distance between two points. This property can be exploited to reduce the computational cost to $\mathcal{O}(N)$ by introducing spatially-localized orbitals and by truncating the elements of the density matrix that belong to atoms distant more than a given cut-off radius[9,10]. Codes such as ONETEP[11], CONQUEST[12], SIESTA[13] and OPENMX[14] belong to this category of linear-scaling methods and are capable to perform calculations on thousands of atoms[15].

The ground state of the system is found by Self-Consistent Field (SCF) minimization of the energy with respect to a number of variational parameters[16]. The Hellmann-Feynman theorem[17,18] provides a computationally-efficient method to calculate the forces acting on ions at the ground state of the system that eliminates the need to calculate the derivatives of the variational parameters describing the orbitals. While this theorem holds for SCF solutions in the limit of a complete basis set[19–21], practical computational approaches to DFT employ a finite number of basis set functions with a certain degree of incompleteness. In such cases, Pulay forces[22] must be calculated as corrections to the Hellmann-Feynman forces if the basis set functions explicitly depend on the ionic positions. Other approaches[23] propose to place the localized orbitals in the centroid of charge of the orbitals that minimize the total energy, so that when self-consistency is achieved, Pulay forces vanish.

Different choices of localized atomic orbitals centered in the atomic coordinates include analytical functions such as Gaussian[24,25] or Slater-type[26] orbitals and numerical representations such as all-electron Numerical Atomic Orbitals (NAOs)[27,28] or Pseudo-Atomic Orbitals (PAOs)[29–33] to account for the valence electrons. Schemes were a combination of plane waves and Gaussian localized orbitals have also been developed[34–37].

In these methods, the quality of the basis set is controlled by the number of functions

for each atomic shell (multiple-zeta basis sets) and the symmetry inherent to the angular momenta of those functions, which leads to polarization and diffuse orbitals which are key to describing the electronic structure of a molecular system. A large set of basis functions is normally required to achieve chemical accuracy in the description of the Kohn-Sham ground state. To reduce the number of atomic orbitals without decreasing the accuracy, a minimal-size set of localized orbitals can be optimized *in situ* in terms of a systematically convergable basis set[38] that removes the restriction of fixed angular shape.

In this work we show that Pulay forces must be calculated in cases where the localized orbitals are optimized in terms of a basis set independent of the ionic coordinates. Geometry optimizations carried on with corrected forces show improved systematic convergence with the basis set and lead to more accurate results. Additionally, Pulay forces are necessary in the more conventional case where the localized orbitals remain constant. In some cases, especially for large systems, geometry optimization calculations with fixed multiple-Z PAO basis set can result in faster time-to-solution runtimes while retaining high accuracy in the final geometries.

We have implemented the functionality that allows for calculation of Pulay forces within the ONETEP[11] code for linear-scaling DFT calculations. Section II offers a brief description of the SCF minimization of the energy and the conditions that are met at convergence of the calculations. In Section III we elaborate on the evaluation of the ionic forces and the origin of the Pulay forces as a consequence of the localization constraints. In Section IV we first show our results regarding the convergence of the total forces in ONETEP, including the Pulay forces, with respect to the basis set for a CO_2 molecule and a water dimer complex and we demonstrate that the Pulay term does not vanish when the localized orbitals are optimized *in situ* with respect to a position-independent basis set. To validate our method, we performed geometry optimization calculations on an adenine-thymine DNA base pair and on the self-assembling superstructure known as the "tennis-ball" dimer[39,40], and we show how the cost of the calculation can be reduced by using fixed multiple-zeta PAO basis sets while retaining accurate results compared to the calculations with optimized localized orbitals. As an application to large-scale systems, we performed geometry optimization calculations on a DNA fragment of 1045 atoms.

II. ENERGY MINIMIZATION

ONETEP[11] is based on a reformulation of Kohn-Sham DFT with norm-conserving pseudopotentials[41] in terms of the single-particle density matrix, $\rho(\mathbf{r},\mathbf{r}')$, represented in a set of Non-Orthogonal Generalized Wannier Functions (NGWFs)[42], $\phi_\alpha(\mathbf{r})$, as:

$$\rho(\mathbf{r},\mathbf{r}') = \phi_\alpha(\mathbf{r}) K^{\alpha\beta} \phi^*_\beta(\mathbf{r}') \tag{1}$$

where the notation assumes implicit summation over repeated Greek indexes and $K^{\alpha\beta}$ are the elements of the density kernel, that is, the representation of ρ in terms of the NGWFs. To achieve linear-scaling cost, the elements of the density kernel corresponding to atoms distant more than a given cut-off radius r_K are truncated. The cut-off radius is chosen so that it is compatible with the exponential decay of ρ in non-metallic systems, resulting on K being a sparse matrix with non-zero elements close to the diagonal[43]. At the same time, the NGWFs are centered on the nuclear coordinates and strictly localized within a sphere of radius R_α, and define the overlap matrix:

$$S_{\alpha\beta} = \int d\mathbf{r}\, \phi_\alpha(\mathbf{r}) \phi^*_\beta(\mathbf{r}) \tag{2}$$

The NGWFs are expanded as a linear combination of psinc functions[44], $D_m(\mathbf{r})$, as:

$$\phi_\alpha(\mathbf{r}) = \sum_{m}^{m\in LR(\alpha)} D(\mathbf{r}-\mathbf{r}_m) c_{m\alpha}, \tag{3}$$

where m indexes the points of the real-space Cartesian grid $\mathbf{r}_m$ inside the localization region of ϕ_α, $LR(\alpha)$. The psinc functions form an orthogonal basis set of bandwidth-limited delta functions related to plane-waves by a unitary transformation, and hence they share many of the desirable properties of these, notably the independence on the nuclear coordinates and the ability of the basis set to be systematically improved by increasing a single parameter: the kinetic energy cut-off[41]. The total energy is minimized self-consistently with respect to $K^{\alpha\beta}$ and $c_{m\alpha}$ in two nested loops[42,45], subject to the constraints of conservation of the total number of electrons and idempotency of the density kernel. The first constraint is enforced by ensuring $tr[KS] = N_e$ during the energy minimization, while idempotency is enforced using the Li-Nunes-Vanderbilt (LNV) method[46] which preserves the orthonormality

of the Kohn-Sham states at zero electronic temperature. As a result, the converged solution satisfies:

$$\frac{\partial E}{\partial K^{\alpha\beta}} = 0 \ \forall \ \alpha, \beta, \tag{4}$$

and

$$\frac{\partial E}{\partial c_{m\alpha}} = 0 \ \forall \ m, \alpha. \tag{5}$$

We emphasize that the NGWFs are optimized *in situ* based on the variational principle. The condition in Eq. (5) refers to the stationarity of the energy with respect to the NGWFs expressed in the psinc representation.

An alternative approach to self-consistent energy minimization is to instead employ a single loop that optimizes the elements of the density kernel only. In this approach, the basis set comprises localized orbitals which remain fixed during the calculation. A recent addition to ONETEP allows generation of suitable multiple-zeta basis sets out of pseudoatomic orbitals (PAOs), and can also be used with high accuracy given a large enough basis. The PAOs are closely related to the Sankley-Niklewski "fireballs"[29] under strict localization constraints. The PAO solver is described in the Appendix.

It should be emphasised that NGWFs differ from the PAOs in that they are expressed and optimized *in situ* in terms of a linear combination of psinc basis functions, whereas the PAOs, although they are also expressed in terms of psinc for consistency throughout, remain fixed. Hence, the condition of Eq. (5) never holds for PAOs.

III. IONIC FORCES

The evaluation of the ionic forces in ONETEP has been previously studied in Ref. 47 for calculations using NGWFs. The force on each ion is defined as the negative total derivative of the system energy with respect to the coordinates of the nucleus of that ion. Explicit derivatives of the elements of the density kernel, $K^{\alpha\beta}$, and the coefficients of the NGWFs in terms of the psinc functions, $c_{m\alpha}$, enter the equation of the forces:

$$\begin{aligned} \mathbf{F}_{\gamma} = -\frac{dE}{d\mathbf{R}_{\gamma}} = &-\frac{\partial E}{\partial \mathbf{R}_{\gamma}} - \frac{\partial E}{\partial K^{\beta\alpha}} \frac{\partial K^{\alpha\beta}}{\partial \mathbf{R}_{\gamma}} \\ &- \int d\mathbf{r} \frac{\delta E}{\delta \phi_{\alpha}(\mathbf{r})} \frac{\partial \phi_{\alpha}(\mathbf{r})}{\partial \mathbf{R}_{\gamma}}. \end{aligned} \tag{6}$$

where $\frac{dE}{d\mathbf{R}_\gamma}$ is the total derivative of the energy with respect to the nuclear coordinates, and includes its *explicit* dependency (first term in the right-hand side) and its *implicit* dependency via the variational parameters (last two terms in the right-hand side). When a tight convergence of the SCF energy minimization is achieved, the conditions in Equations (4) and (5) apply, so the *implicit* derivatives of the energy with respect to $K^{\alpha\beta}$ and $c_{m\alpha}$ vanish, leaving a much simpler expression for the total force:

$$\mathbf{F}_\gamma = -\frac{\partial E}{\partial \mathbf{R}_\gamma}. \tag{7}$$

This result corresponds to direct application of the Hellmann-Feynman theorem after successful SCF energy minimization, with vanishing Pulay forces. The total Hellmann-Feynman force on atom γ is formed by individual contributions to the Hamiltonian, and does not consider derivatives of the NGWFs themselves. It thus includes local and non-local pseudopotential, Ewald, and (where applicable) non-linear core correction (NLCC) terms:

$$\mathbf{F}_\gamma^{\mathrm{HF}} = \mathbf{F}_\gamma^{\mathrm{nl}} + \mathbf{F}_\gamma^{\mathrm{loc}} + \mathbf{F}_\gamma^{\mathrm{ew}} + \mathbf{F}_\gamma^{\mathrm{nlcc}}. \tag{8}$$

Eq. (8) will remain valid when the condition in Eq. (5) holds. However, obtaining tight convergence of energy with respect to the psinc coefficients can be very difficult, due to the competition between the kinetic energy operator, which tends to spread the NGWFs across the cell, and the constraint of strict localization of the NGWFs within a sphere[48]. In such circunstances the NGWF energy gradient in psinc representation tends to converge to small non-zero values. Whereas the total energy converges quadratically with respect to the Kohn-Sham states during the SCF procedure, the forces converge at a slower rate[22]. As a result, the residual NGWF energy gradient has a negligible effect in the evaluation of the ground-state energy, yet can produce non-negligible Pulay corrections to the Hellmann-Feynman forces. The methodology implemented in ONETEP for density kernel optimization based on the Li-Nunes-Vanderbilt algorithm[45,46] allows to converge the energy with respect to $K^{\alpha\beta}$ to a very tight tolerance, so that the condition in Eq. (4) is achieved. Therefore, the Pulay forces term is due entirely to the NGWF contribution in Eq. (6):

$$\mathbf{F}_\gamma^{\mathrm{Pulay}} = \int d\mathbf{r} \frac{\delta E}{\delta \phi_\alpha(\mathbf{r})} \frac{\partial \phi_\alpha(\mathbf{r})}{\partial \mathbf{R}_\gamma}. \tag{9}$$

For a given set of localized functions and density kernel, the total force on atom γ at the

Kohn-Sham ground state is the sum of the Hellmann-Feynman forces and the Pulay forces: $\mathbf{F}_\gamma^{\text{total}} = \mathbf{F}_\gamma^{\text{HF}} + \mathbf{F}_\gamma^{\text{Pulay}}$.

The above expression is valid for any set of localized functions. As the PAOs are also represented as a linear combination of psinc functions, the method presented hereafter for determining Pulay forces holds for both NGWFs and PAOs. As seen from Eq. (9), the Pulay forces require evaluation of two terms and integration of their product on a real space grid within the localisation region of the relevant NGWF: the energy gradient with respect to the NGWFs and the derivative of the NGWFs with respect to the ionic coordinates. The first is evaluated at each step of the SCF optimization of the NGWFs and does not need to be recalculated to evaluate the forces. This makes the computation of Pulay forces inexpensive compared to the SCF cycle, which takes most of the computational effort. The analytical form of $\frac{\delta E}{\delta \phi_\alpha(\mathbf{r})}$ has been derived before by Soler *et al.*[13] for a generalized Lagrangian to keep orthogonality of the Kohn-Sham states and Miyazaki *et al.*[49] for the LNV method. The expression is equivalent in the case of ONETEP:

$$\frac{\delta E}{\delta \phi_\alpha(\mathbf{r})} = 4\left[\hat{H}\phi_\beta(\mathbf{r})K^{\beta\alpha} + \phi_\beta(\mathbf{r})Q^{\beta\alpha}\right], \tag{10}$$

where, for a converged density kernel, $Q^{\alpha\beta} = -(KHS^{-1})^{\alpha\beta}$. The prefactor of 4 in Eq. (10) appears as the NGWFs are real functions and closed shells are assumed. On the other hand, derivatives with respect to the ionic coordinates can be calculated by applying the gradient operator to the NGWFs:

$$\frac{\partial \phi_\alpha(\mathbf{r})}{\partial \mathbf{R}_\gamma} = -\nabla_{\mathbf{r}}\phi_\alpha(\mathbf{r})\delta_{\alpha\gamma}. \tag{11}$$

The gradient operator acts on the reciprocal space representation of the function $\phi_\alpha(\mathbf{r})$ using the well-tested FFT-box technique[44]. The equivalence of the psinc functions and plane waves allow us to expand Eq. (3) as:

$$\phi_\alpha(\mathbf{r}) = \frac{1}{N_p}\sum_{\mathbf{G}}^{\mathbf{G}_{\max}} \tilde{\phi}_\alpha(\mathbf{G})e^{i\mathbf{G}(\mathbf{r}-\mathbf{R}_\alpha)} \tag{12}$$

where $\mathbf{G}$ denotes the reciprocal lattice vectors on the FFT-box up to a magnitude of $\mathbf{G}_{\max}$, defined by the kinetic energy cut-off. N_p indicates the number of points in the FFT-box, whose size is proportional to the NGWF radii. It necessary to stress that the dependency of $\phi_\alpha(\mathbf{r})$ on $\mathbf{R}_\alpha$ does not involve a change in the functional form of the NGWFs as expressed

in terms of the psinc basis set, but instead it remains as a translational phase factor that takes into account the displacement of the NGWF center across the simulation cell. Direct differentiation of Eq. (12) provides the derivative of the NGWFs with respect to $\mathbf{R}_\gamma$:

$$\frac{\partial \phi_\alpha(\mathbf{r})}{\partial \mathbf{R}_\gamma} = \frac{1}{N_p} \sum_{\mathbf{G}}^{\mathbf{G}_{\max}} -i\mathbf{G}\tilde{\phi}_\alpha(\mathbf{G}) e^{i\mathbf{G}(\mathbf{r}-\mathbf{R}_\alpha)} \delta_{\alpha\gamma}. \tag{13}$$

Equations (10) and (13) are evaluated in the FFTbox of ϕ_α so that $\mathbf{F}_\gamma^{\text{Pulay}}$ can be calculated with $\mathcal{O}(N)$ cost.

IV. RESULTS

A. Convergence of the forces

Convergence with respect to the psinc basis set (cut-off energy) and the radius of the spherical localization region of the NGWFs is vital for accurate calculation of ionic forces within this method. This aspect has been studied in Ref. 47 for the Hellmann-Feynman forces alone, with results presented for the force on an oxygen atom in CO_2 and the force on a hydrogen atom in a H_2O dimer. Fig. 1 reproduces these results and additionally demonstrates the effect of the Pulay correction to the total forces. These calculations used the LDA exchange-correlation functional, employing one NGWF for hydrogen and four for carbon and oxygen atoms.

The total forces, calculated as the sum of the Hellmann-Feynman components and the Pulay corrections, converge to a single value as the cut-off energy and NGWF radii increase, and are comparable to the values obtained with CASTEP plane-wave DFT. Adding the Pulay correction term to the Hellmann-Feynman forces ensures a greater degree of consistency between ground-state energies and forces in the calculations performed with ONETEP. Pulay forces take a non-negligible value for small localization regions and converge to zero when the NGWFs become larger and more delocalized. The Pulay corrections do not vanish as the cut-off energy increases, showing the strong correlation with the localization constraint. The relative strength of the Pulay correction compared to the Hellmann-Feynman force is greater in the case of the hydrogen bond in the water dimer (up to 15% of the Hellmann-Feynman value) than in the covalent bond of CO_2 (3%). Therefore, Pulay forces can be expected to play a more significant role in the ionic forces of weakly bonded systems, particularly when

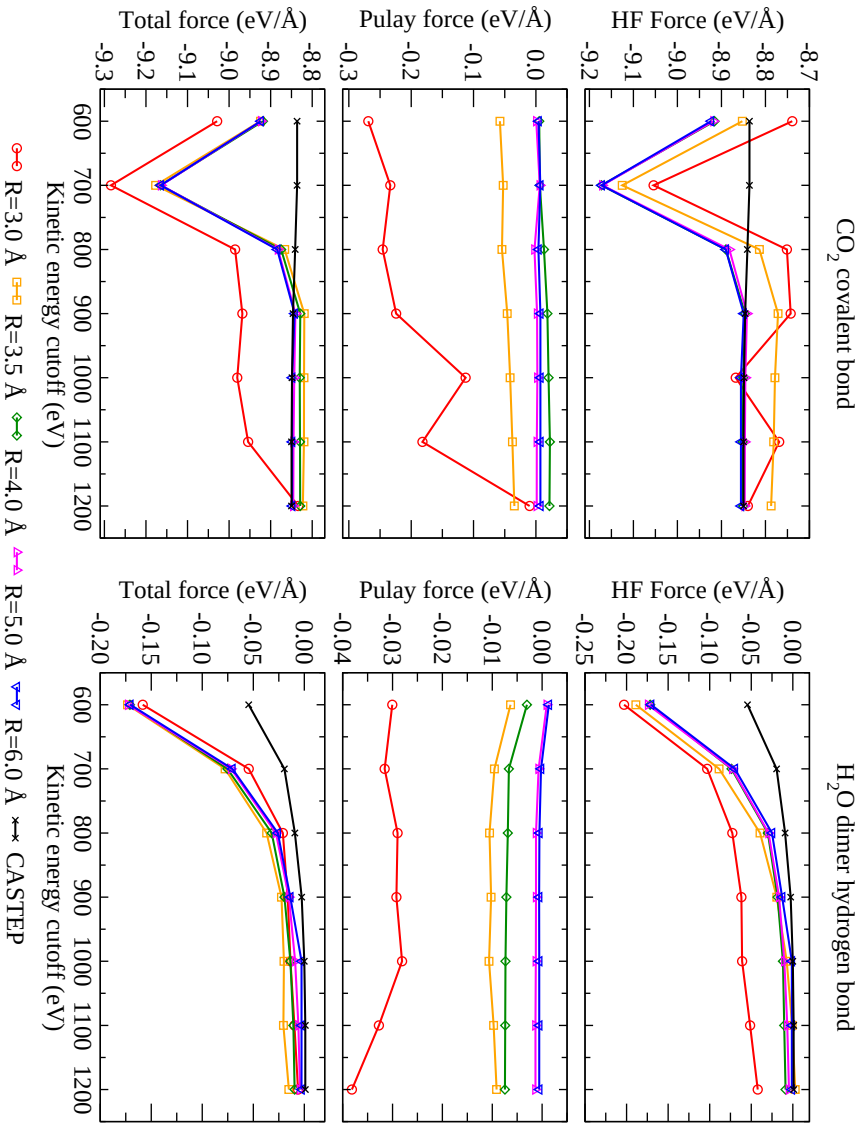

Figure 1. Convergence of the forces with respect to the cut-off energy and the NGWF radius. Left: force in an oxygen atom in CO_2 along the covalent bond. Right column: force on a hydrogen atom in H_2O dimer along the hydrogen bond. The first row corresponds to the Hellmann-Feynman force, the second to the Pulay force and the third are the Pulay-corrected total forces (Hellmann-Feynman forces plus Pulay). R refers to the NGWF radii.

modelled with small NGWF radii.

Real-space grid methods can suffer of the so-called egg-box effect[50,51], which appears when the localized orbitals are displaced by a fraction of the grid-spacing in the simulation cell generating periodic oscillations of the converged ground-state energy and forces. An estimation of the egg-box effect in the total energy and the forces is shown in Fig. 2. These

calculations consecutively displace a CO_2 molecule along the first axis of the simulation cell (parallel to the CO_2 covalent bond) by a given step of 1/20 of the grid spacing of 0.24 Å. We use the PBE exchange-correlation functional[52] with a kinetic energy cut-off of 1000 eV and NGWF radii of 4.23 Å to ensure convergence of the forces with the basis set. SZ, DZP and TZDP basis sets were constructed using PAOs as described in the Appendix . The magnitude of the egg-box effect is reduced when NGWFs are used instead of PAOs contributing to more stability in calculations where the ionic coordinates vary, such as geometry optimization. The maximum variation of the energy using NGWFs is of 1.6×10^{-3} eV, which is up to ten times smaller compared to SZ calculations. NGWFs also reduce the magnitude of the egg-box effect on the forces to 0.01 eV/Å, nearly a third of the magnitude in the case of SZ calculations.

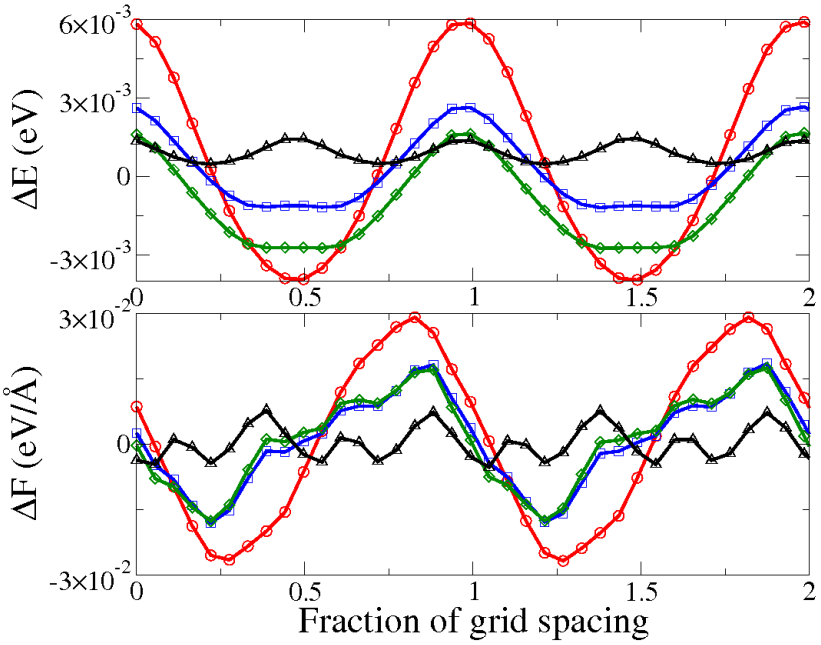

Figure 2. Eggbox effect on the energy (top) and force along covalent bond (bottom) on CO_2 with SZ/PAOs (red circles), DZP/PAOs (blue squares), TZDP/PAOs (green diamonds) and NGWFs (black triangles). The energy cut-off is 1000eV and the PAO and NGWF radii is 4.23 Å.

B. Geometry optimization using NGWFs

We have performed geometry optimization calculations using the BFGS algorithm[53] in ONETEP to test the accuracy of the force evaluation in practical applications. Calculations

on an adenine-thymine DNA base pair were carried out as a first test case. This system is weakly bound by two hydrogen bonds that involve oxygen and nitrogen making it more challenging for self-consistent minimization of the total energy and forces. PBE[52] calculations with 1200 eV kinetic energy cut-off and various NGWF radii were performed with uncorrected Hellmann-Feynman forces and Pulay-corrected forces, using one NGWF for the hydrogen atoms and four for oxygen, carbon and nitrogen. We compared the resulting structures with those given bt NWChem with a cc-pVTZ Gaussian basis set and Castep with the same plane-wave cut-off and pseudopotentials as Onetep. The results are shown in Table I.

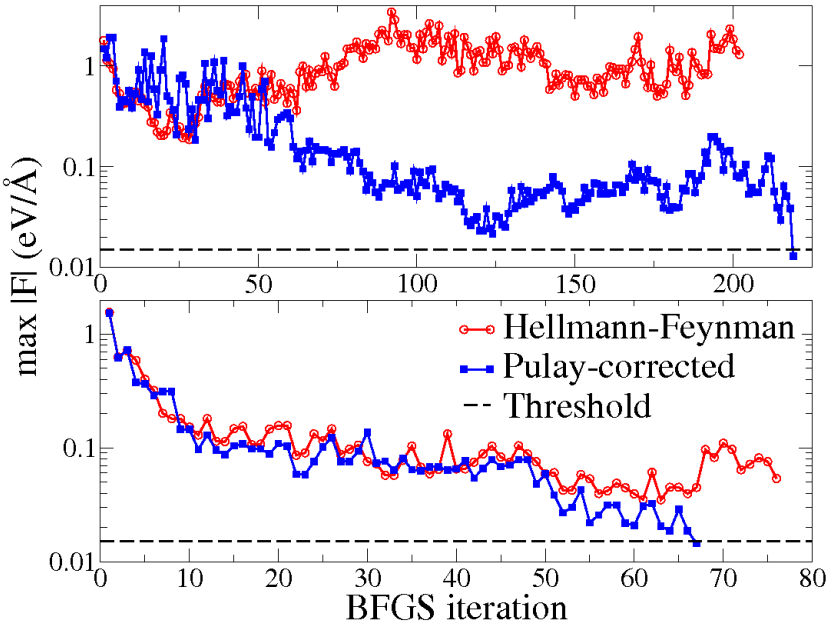

Figure 3. Convergence of the maximum absolute value of the force during geometry optimization of the adenine-thymine DNA base pair with NGWF radii of 3.70 Å (top) and 7.94 Å (bottom). The convergence threshold was 0.015 eV/Å.

The addition of Pulay corrections to the Hellmann-Feynman forces improves the convergence of the BFGS algorithm for all the range of NGWF radii, having a more important effect for small localization regions, where it allows relaxation of the structure to much tighter tolerance thresholds. The calculations using uncorrected Hellmann-Feynman forces with small NGWF radii result in poor description of hydrogen bonding in the adenine-thymine complex, leading to heavily distorted geometry and to unphysical configurations. In the uncorrected case, increasing the NGWF radius eventually results in a bound and

Table I. Geometry optimization of adenine-thymine using ONETEP for different localization radii R_α with Hellmann-Feynman forces (HF) and Pulay-corrected forces (PC). Results show the hydrogen bond lengths, the maximum absolute value of the force, $|F|_{\max}$, and the number of BFGS steps required.

		O...H bond (Å)		N...H bond (Å)		$\|F\|_{\max}$ (eV/Å)		BFGS steps	
	R_α (Å)	HF	PC	HF	PC	HF	PC	HF	PC
ONETEP	3.70	9.77	1.73	10.64	1.60	1.028	0.010	203	222
	4.23	5.39	1.75	7.15	1.62	1.542	0.015	128	73
	4.86	1.90	1.80	1.65	1.65	1.542	0.015	80	73
	5.39	1.61	1.83	1.62	1.69	0.514	0.015	95	90
	5.82	1.73	1.83	1.64	1.71	1.028	0.015	100	63
	6.45	1.75	1.83	1.57	1.72	0.463	0.015	92	63
	6.98	1.85	1.84	1.62	1.72	0.463	0.015	97	65
	7.41	1.81	1.84	1.68	1.73	0.206	0.015	92	74
	7.94	1.83	1.84	1.67	1.73	0.051	0.015	78	69
NWCHEM	—	1.84		1.73		0.026		102	
CASTEP	—	1.85		1.75		0.010		88	

symmetric system, albeit the maximum value of the residual force remains higher than in the corrected case after a similar number of BFGS steps. The convergence of the maximum element of the force is plotted in Fig. 3. This demonstrates that accuracy in the force evaluation is crucial to enabling the BFGS method to find the equilibrium geometry of the system. Our results also show that the geometry of the adenine-thymine complex after relaxation with Pulay-corrected forces is still somewhat sensitive to the NGWF radius. Overly-small NGWF localization regions tend to overbind the hydrogen bonds, while as radii increase, the geometry converges to the expected structure as given by NWCHEM and CASTEP.

We have used the geometry obtained with each method to calculate the binding energy of the adenine-thymine complex, calculated as $E_{\text{complex}} - E_{\text{adenine}} - E_{\text{thymine}}$, where the first term is the energy of the geometry-optimized complex and the last two are the energies of each separate monomer with the same geometry as in the complex. The results in Fig. 4

show systematic convergence with respect to the localization radius when the Pulay forces are taken into account, while, in contrast, the calculations using Hellmann-Feynman lead to extreme variations and erratic convergence. In this case, the binding energies obtained with Pulay-corrected forces converge within 1 kcal/mol for NGWF radii larger than 5.5 Å. Nevertheless, the convergence of these set of calculations is due to simultaneous change of the basis set (increasing NGWF radii) and of the final structure. To isolate the convergence of the binding energies with respect to the basis set we chose the structures obtained for 3.70 and 7.94 Å (Pulay-corrected) and re-calculated the binding energies for different NGWF radii. In these calculations the binding energy converges within 1 kcal/mol for NGWF radii larger than 4.2 Å. Basis set superposition error is eliminated due to the optimization of the NGWFs in terms of the psinc basis set[54].

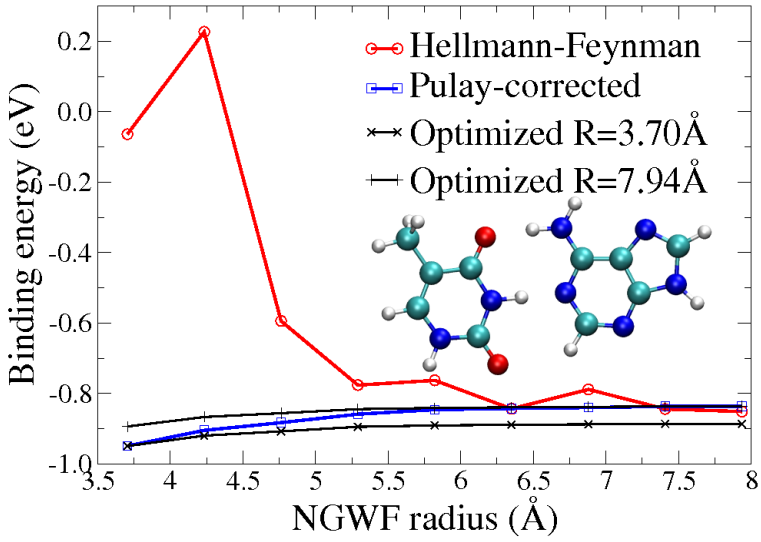

Figure 4. Convergence of the binding energy in the Adenine-Thymine complex.

We have also performed geometry optimization calculations in the larger system of the "tennis-ball" self-assembling superstructure[39,40], which is a model for protein-ligand binding interactions. This molecule is formed by two identical structures that bind each other when rotated 90 degrees via eight hydrogen bonds. The calculations, performed with the PBE[52] functional, 1200 eV energy cut-off and one NGWF per hidrogen atom and four per oxygen, nitrogen and carbon atoms with NGWF radius of 3.70 Å, show that in the absence of Pulay

forces, the system loses its symmetry and eventually breaks (Fig. 5), while the minimization of the force is unstable and highly oscillating. When the Pulay forces are included the BFGS method converges to a symmetric structure and a low threshold of force tolerance (0.015 eV/Å).

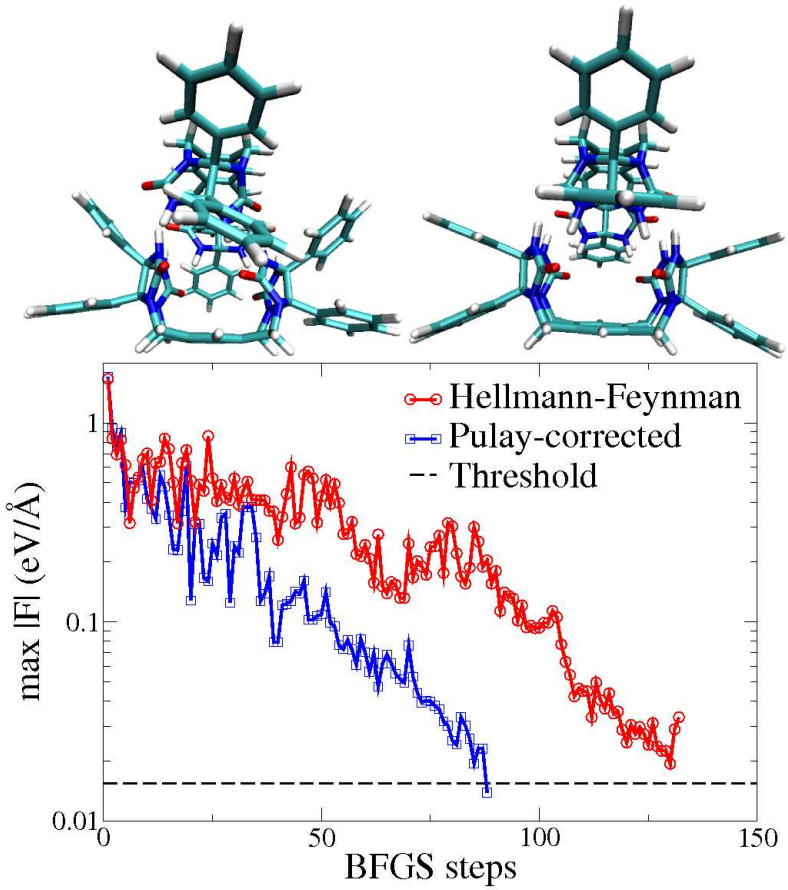

Figure 5. Convergence of the maximum force during the BFGS geometry optimization of the tennis-ball dimer using Hellmann-Feynman forces (top left molecule) and Pulay-corrected forces (top right).

C. Geometry optimization using PAOs

Geometry optimization calculations using PAO multiple-zeta basis sets have been performed on the adenine-thymine DNA base pair, using the same exchange-correlation functional, pseudopotentials and cut-off energy than in the case of NGWFs. The results, shown in Table II, are consistent with those obtained with NGWFs for the same radii, and calcula-

tions with medium-size basis sets such as TZP, TZDP or QZP are thus also seen to converge to the same structures obtained with NWChem and Castep in Table I.

Table II. Lenth of the two Hydrogen bonds in the DNA pair adenine-thymine for different PAO radii R. Onetep calculations use a plane wave basis set of 1200 eV and forces converged to 0.015 Å.

	O...H bond (Å)			N...H bond (Å)		
R (Å)=	3.70	4.23	4.86	3.70	4.23	4.86
SZ	1.41	1.42	1.42	1.32	1.31	1.31
SZP	1.57	1.61	1.56	1.32	1.31	1.31
DZ	1.66	1.67	1.65	1.49	1.52	1.53
DZP	1.74	1.73	1.71	1.58	1.58	1.57
TZ	1.70	1.71	1.69	1.53	1.58	1.56
TZP	1.83	1.84	1.81	1.68	1.69	1.68
TZDP	1.79	1.84	1.79	1.68	1.68	1.68
QZ	1.73	1.71	1.71	1.55	1.56	1.57
QZP	1.81	1.82	1.81	1.67	1.66	1.69

D. Geometry optimization in large systems

As an example of the applicability of the aforementioned methods to large-scale systems, we performed a geometry optimization calculation on a DNA fragment of 16 base pairs and 1045 atoms in vacuum. The initial structure was created using Amber Nucgen[55] (sequence ATCGATTGAGCTCTAG) and the phosphate groups were protonated so that the total charge is zero. The calculations were run using the PBE exchange-correlation functional[52] and a kinetic energy cut-off of 1200 eV, using, for each case, NGWFs (one for hydrogen atoms, four for oxygen, nitrogen and carbon, and nine for phosphorus), DZP and TZP PAO basis sets of radii of 3.70 Å. The convergence threshold for the force was set to 0.16 eV/Å. This can be considered high for conventional quantum chemical standards, while it has been chosen as to account for the non-monotonic convergence of the BFGS algorithm

to the equilibrium geometry due to the large count of atoms in this system. Fig. 6 shows convergence of the force for the different calculations, while Table III shows some structural parameters mand the change underwent through the geometry optimization.

The maximum value of the force converges in all cases. The final structure given by DZP possesses clear differences with respect to TZP and NGWFs: shorter length, smaller radius and much shorter hydrogen bonds formed on each base pair. This observation is in agreement with the results of the adenine-thymine single base pair, in which the DZP basis set tends to overbind hydrogen bonds. TZDP and optimized NGWFs offer more similar results.

Noticeably, the calculation with NGWFs requires fewer steps to complete in comparison with DZP and TZDP PAO basis sets. This is likely to be a consequence of the more accurate description of the Kohn-Sham ground-state provided by the NGWF optimization. Similarly, TZDP also requires fewer steps than DZP due to its better degree of completeness. For the basis sets used in this study, each BFGS step is completed somewhat faster when using PAOs, as overall fewer matrix operations are required due to the absence of the outer loop required for NGWF optimisation. As a reference, the calculations were run using 15 Intel Nehalem nodes with 8 cores each, making it a total of 120 processors. The average BFGS step took 3.2 hours with the DZP PAO basis set, 7.6 hours with TZDP PAO basis set, and 8.3 hours with the NGWFs optimized in the psinc basis set. This reduction overcomes the increasing cost of algebraic operations with more basis set functions and thus larger matrices.

V. CONCLUSIONS

In this work we have shown that the Pulay forces correction to the Hellmann-Feynman forces must be calculated for accuracy in the in total ionic forces. Using localized orbitals optimized *in situ* in terms of a basis set that is independent of the nuclear positions, such as psinc functions, does not eliminate the Pulay forces. This is due to the tendency of the kinetic energy gradient to delocalize the atomic orbitals which are constrained to be stricly localized within a sphere of finite radius. The implementation in ONETEP ensures consistency between the Pulay-corrected forces and the energy calculated self-consistently.

Geometry optimization calculations, which heavily rely upon accurate ionic forces, prove

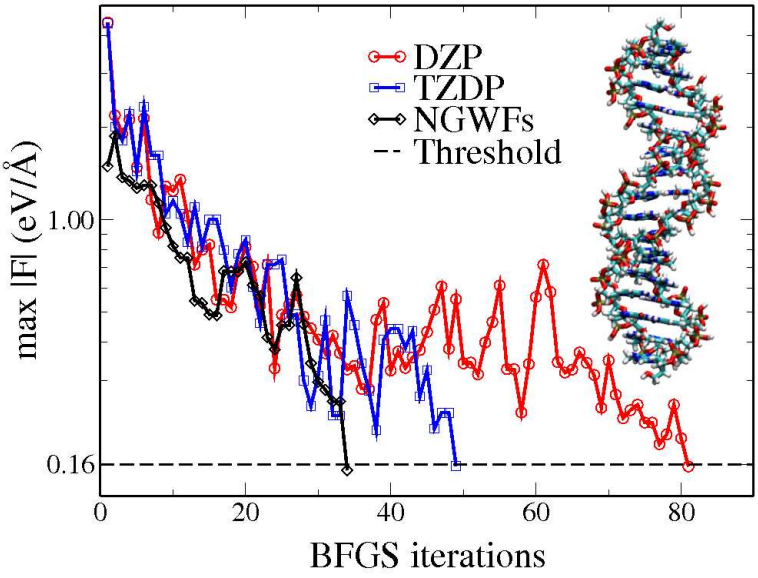

Figure 6. Convergence of the maximum force for the DNA molecule using optimized NGWFs and frozen DZP and TZDP PAO basis sets.

to yield to much better results when Pulay forces are taken into account. Molecular systems containing weakly-bound components are better described by the inclusion of Pulay forces. Our method can be used for large-scale geometry optimization calculations on systems of more than a thousand atoms, with the results being systematically convergable with respect to the basis set.

The Pulay forces corrections also allow calculations in which the localized orbitals are fixed during the calculation. PAO are reliable and convergable method to construct suitable multiple-zeta basis sets of increasing accuracy. Calculations with medium-sized PAO basis sets can offer faster runtimes allowing to perform costly calculations such as geometry optimization on large systems. This is due to the reduction of the matrix operations as the outer loop to optimize the localized orbitals is avoided, which overcomes the extra cost due to algebraic operations with larger matrices.

ACKNOWLEDGMENTS

A.R.S. acknowledges the support of the Engineering and Physical Sciences Research Council (EPSRC) (Grant No EP/F038038/1) for a High End Computing Studentship

Table III. Structural parameters of the optimized 1045-atom DNA fragment as optimized by ONETEP. N...H(4), N...H(8) and N...H(12) correspond to the hydrogen bond of the fourth, eighth and twelfth pairs, respectively, that involve a nitrogen atom.

Basis set	DZP		TZDP		NGWFs	
	Final	Change	Final	Change	Final	Change
Length (Å)	49.74	−1.18	50.62	−0.35	50.50	−0.47
Diameter (Å)	15.31	0.04	15.32	0.05	15.21	−0.06
Helix pitch (Å)	24.05	0.34	23.63	0.08	23.55	0.16
NH(4)	1.66	−0.21	1.78	−0.09	1.80	−0.07
NH(8)	1.48	−0.33	1.62	−0.19	1.67	−0.14
NH(12)	1.54	−0.27	1.63	−0.18	1.64	−0.17

through the UKCP consortium. N.D.M.H. acknowledges the support EPSRC (Grant No EP/G05567X/1) for postdoctoral funding through the HPC Software Development call 2008/2009. C.-K.S. acknowledges support from the Royal Society in the form of a University Research Fellowship. The authors are grateful for the computing resources provided by Southampton University's iSolutions unit (Iridis3 supercomputer) which have enabled all the calculations presented here.

Appendix: Pseudoatomic Solver

1. Generating Valence PAOs

Initial NGWFs can be generated by performing a Kohn-Sham DFT calculation for a pseudoatom. The pseudopotential of a single isolated ion provides the external potential, and the single-electron Kohn-Sham states are solved self-consistently at fixed occupancies. The resulting states form an ideal pseudoatomic orbital basis for calculations on molecules or solids with the same choice of pseudopotential and functional.

The PAOs are solutions of the Kohn-Sham equation:

$$\left(-\frac{1}{2}\nabla^2 + V_{\rm loc}(r) + \hat{V}_{\rm nl}\right)|\psi_{nlm}\rangle = \epsilon_{nl}|\psi_{nlm}\rangle \tag{A.1}$$

where the Hamiltonian contains kinetic, local effective potential and nonlocal potential contributions for an isolated atom in spherical confinement.

The solutions to this spherically-symmetric problem comprise real spherical harmonics $Z_{lm}(\theta, \varphi)$ multiplying a radial part described by a basis of normalised spherical Bessel functions $B_{l,\nu}(r)$ of given angular momentum l. This choice has been made in other implementations of similar methods[29–31]. The basis functions are defined by

$$B_{l,\nu}(r) = j_l(q_{l,\nu}r) \,/\, \Big[\int_0^{R_c} |j_l(q_{l,\nu}r)|^2 r^2 dr \Big]^{\frac{1}{2}} , \tag{A.2}$$

with $q_{l,\nu}$ chosen such that $q_{l,\nu}R_c$ are the zeros of the spherical Bessel functions $j_l(x)$. This ensures that all the basis functions go to zero at the cutoff radius R_c, which is chosen to coincide with the NGWF cutoff R_α. Furthermore, $\int_0^{R_c} |B_{l,\nu}(r)|^2 r^2 dr = 1$ for all ν. The basis is made finite by including only functions with a kinetic energy less than a cutoff energy $E_{\rm cut}$. The criterion $\frac{1}{2}q_{l,\nu}^2 < E_{\rm cut}$ determines the largest ν for each l.

We therefore write the PAO $\psi_{nlm}(\mathbf{r})$ in terms of coefficients $c_{nl,\nu}$ for each basis function, in the form

$$\psi_{nlm}(\mathbf{r}) = \sum_\nu c_{nl,\nu}\, B_{l,\nu}(r)\, Z_{lm}(\theta\varphi) \,, \tag{A.3}$$

with eigenvalues ϵ_{nl} and occupancies f_{nl} (which account for spin-degeneracy). The occupancies are fixed such that they obey the aufbau principle and sum to the number of valence electrons. Spherical symmetry means that the occupancies of all members of a given set of m-degenerate orbitals are equal, so we combine the $2l+1$ degenerate states of differing m for a given nl state into one state to be solved with the sum of the occupancies of the shell. Henceforth we will only consider the radial dependence $R_{nl}(r)$.

We define the local potential to be

$$V_{\rm loc}(r) = V_{\rm psloc}(r) + V_H(r) + V_{XC}(r) + V_{\rm conf}(r) \tag{A.4}$$

where the Hartree and XC terms are included in the standard way, as is an optional confining potential implemented as described in Ref. 28.

For each value of l we can define the Hamiltonian and overlap matrices

$$H^l_{\nu,\nu'} = \int_0^{R_c} B_{l,\nu}(r) \left[\hat{H} B_{l,\nu'}(r)\right] r^2 dr \tag{A.5}$$

and

$$S^l_{\nu,\nu'} = \int_0^{R_c} B_{l,\nu}(r) B_{l,\nu'}(r) r^2 dr \tag{A.6}$$

and solve the secular equation

$$\mathbf{H}^l.\mathbf{c}_{nl} = \epsilon_{nl}\mathbf{S}^l.\mathbf{c}_{nl} \tag{A.7}$$

to give the coefficients $c_{nl,\nu}$ describing the orbitals. The orbitals are then evaluated on a regular radial real-space grid and used to construct the total density. Density mixing with a variable mixing parameter α is then used and the SCF cycle repeats until self-consistency is obtained. The result is deemed to be converged once the Harris-Foulkes[56,57] estimate of the total energy (the bandstructure energy) matches the total energy as determined from the density to within a tolerance of 2.7×10^{-4} eV, and the energy has stopped changing at each iteration to within a tolerance of 2.7×10^{-6} eV.

2. Generating larger basis sets

We follow the procedure described in Ref. 30 for generating larger PAO basis sets, appropriate for calculations with a fixed basis. Briefly, this works in two ways: firstly, the radial flexibility can be improved by splitting each of the valence orbitals into multiple zeta functions. Secondly, the highest-l valence states can be polarised using perturbation theory, to produce orbitals for higher angular momentum values than exist in the valence states.

The former is achieved by setting fractional values N_i of the norm, known as the "splitnorms", which determine matching radii r_m. which are then used to divide the function into components. The matching radius corresponding to each splitnorm is chosen such that the norm from r_m to the cutoff radius R_c is equal to the N_i. Typically, $N_1 \simeq 0.15$ is suitable for most elements. The first new function matches the tail of the original function beyond r_m, and has the form $r^l(a_{i,l} - b_{i,l}r^2)$ for $r < r_m$. The coefficients a_l and b_l are chosen to match the value and gradient at r_m. A second new function is then created by subtracting the new function from the original function and renormalising it. This has the advantage that the second new function is zero beyond r_m and is thus shorter ranged. This procedure can then be repeated on new functions, using new matching radii determined from further splitnorms N_i, where each must be smaller than the last.

Generation of higher angular momentum functions is achieved through perturbation theory, as used extensively elsewhere[13,50]. A valence orbital R_{nl} with eigenvalue ϵ_{nl} is perturbed by an applied electric field in the z direction, $\Delta\hat{V} = \mathcal{E}z$. Perturbation theory then produces

the first-order change in the wavefunction ΔR_{nl} as

$$(\hat{H} - \epsilon_{nl})\Delta R_{nl} = -(\Delta\hat{V} - \Delta\epsilon_{nl})R_{nl} \ . \tag{A.8}$$

Since the perturbation is an odd function of z, the $\Delta\epsilon_{nl}$ term is always zero. The first-order change ΔR_{nl} only contains components with angular momenta $l+1$ and $l-1$, by the dipole selection rule. In most cases we already have angular momentum $l-1$ terms in the basis, so only the $l+1$ term is considered, and the coefficient of this term is dropped as it only affects the normalisation (as does the field strength $\mathcal{E}$).

We can expand the radial part in terms of coefficients d_ν multiplying the basis functions for $l+1$, as

$$\Delta R_{nl}(r) = \sum_\nu d_\nu B_{l+1,\nu}(r) \tag{A.9}$$

Multiplying through by $B_{l+1,\nu'}(r)$ and solving the resulting matrix equation gives us

$$d_\nu = \left(H^{l+1}_{\nu\nu'} - \epsilon_{nl} S^{l+1}_{\nu\nu'}\right)^{-1} D_\nu \ , \tag{A.10}$$

where D_ν is the overlap of the basis functions with the perturbation. After angular integration with $\Delta\hat{V} \propto -r\cos\theta$ this gives

$$D_\nu = -\int_0^{R_c} B_{l+1,\nu}\, r\, R_{nl}(r) r^2 dr \ . \tag{A.11}$$

The resulting wavefunctions (after renormalisation) approximately match the radial weight distribution of the original functions and have the same cutoff. They thus form an ideal extension of the basis, suited to describing the response of the valence states to local electric fields.

The choices of PAO basis set we employed in this work were: Single-Zeta (SZ), with no extra functions beyond the valence orbitals, Double-Zeta (DZ) where the valence states are split into two functions, Double-Zeta plus Polarisation (DZP), where a set of polarisation functions are added, as well as TZ, TZP, TZDP, QZ and QZP, involving three and four basis functions and up to two polarisation shells. SZ is generally regarded as insufficiently accurate for meaningful results, but typically DZP or above can be used for moderately accurate calculations, with TZDP and above providing a well-converged result (albeit at rather high cost).

REFERENCES

[1]P. Hohenberg and W. Kohn, Phys. Rev. **136**, B864 (1964).

[2]W. Kohn and L. J. Sham, Phys. Rev. **140**, A1133 (1965).

[3]M. D. Segall, P. J. D. Lindan, M. J. Probert, C. J. Pickard, P. J. Hasnip, S. J. Clark, and M. C. Payne, J. Phys. Condens. Matter **14**, 2717 (2002).

[4]M. Valiev, E. Bylaska, N. Govind, K. Kowalski, T. Straatsma, H. V. Dam, D. Wang, J. Nieplocha, E. Apra, T. Windus, and W. de Jong, Comput. Phys. Commun. **181**, 1477 (2010).

[5]G. Kresse and J. Furthmüller, Phys. Rev. B **54**, 11169 (1996).

[6]G. te Velde, F. M. Bickelhaupt, E. J. Baerends, C. Fonseca Guerra, S. J. A. van Gisbergen, J. G. Snijders, and T. Ziegler, J. Comput. Chem. **22**, 931 (2001).

[7]P. Giannozzi, S. Baroni, N. Bonini, M. Calandra, R. Car, C. Cavazzoni, D. Ceresoli, G. L. Chiarotti, M. Cococcioni, I. Dabo, A. D. Corso, S. de Gironcoli, S. Fabris, G. Fratesi, R. Gebauer, U. Gerstmann, C. Gougoussis, A. Kokalj, M. Lazzeri, L. Martin-Samos, N. Marzari, F. Mauri, R. Mazzarello, S. Paolini, A. Pasquarello, L. Paulatto, C. Sbraccia, S. Scandolo, G. Sclauzero, A. P. Seitsonen, A. Smogunov, P. Umari, and R. M. Wentzcovitch, J. Phys. Condens. Matter **21**, 395502 (2009).

[8]W. Kohn, Phys. Rev. Lett. **76**, 3168 (1996).

[9]S. Goedecker, Rev. Mod. Phys. **71**, 1085 (1999).

[10]D. R. Bowler and T. Miyazaki, Rep. Prog. Phys. **75**, 036503 (2012).

[11]C.-K. Skylaris, P. D. Haynes, A. A. Mostofi, and M. C. Payne, J. Chem. Phys. **122**, 084119 (2005).

[12]M. J. Gillan, D. R. Bowler, A. S. Torralba, and T. Miyazaki, Comput. Phys. Commun. **177**, 14 (2007).

[13]J. M. Soler, E. Artacho, J. D. Gale, A. Garcia, J. Junquera, P. Ordejon, and D. Sanchez-Portal, J. Phys. Condens. Matter **14**, 2745 (2002).

[14]T. Ozaki and H. Kino, Phys. Rev. B **72**, 045121 (2005).

[15]N. D. M. Hine, P. D. Haynes, A. A. Mostofi, C. K. Skylaris, and M. C. Payne, Comput. Phys. Commun. **180**, 1041 (2009).

[16]A. Szabo and N. S. Ostlund, *Modern Quantum Chemistry. Introduction to Advanced Electronic Structure Theory* (Dover Publications, 1996).

[17]H. Hellmann, Einführung in die Quantenchemie (Deuticke, Leipzig) (1937).

[18]R. P. Feynman, Phys. Rev. **56**, 340 (1939).

[19]A. Hurley, Proc. R. Soc. London, Ser. A **226**, 179 (1954).

[20]M. Scheffler, J. P. Vigneron, and G. B. Bachelet, Phys. Rev. B **31**, 6541 (1985).

[21]M. Di Ventra and S. Pantelides, Phys. Rev. B **61**, 16207 (2000).

[22]P. Pulay, Mol. Phys. **17**, 197 (1969).

[23]J. Fattebert and F. Gygi, Comput. Phys. Commun. **162**, 24 (2004).

[24]E. R. Davidson and D. Feller, Chem. Rev. **86**, 681 (1986).

[25]P. Briddon and R. Jones, Phys. Status Solidi B **217**, 131 (2000).

[26]D. P. Chong, E. Van Lenthe, S. Van Gisbergen, and E. J. Baerends, J. Comput. Chem. **25**, 1030 (2004).

[27]B. Delley, J. Chem. Phys. **92**, 508 (1990).

[28]V. Blum, R. Gehrke, F. Hanke, P. Havu, V. Havu, X. Ren, K. Reuter, and M. Scheffler, Comput. Phys. Commun. **180**, 2175 (2009).

[29]O. F. Sankley and D. J. Niklewski, Phys. Rev. B **40**, 3979 (1989).

[30]E. Artacho, D. Sánchez-Portal, P. Ordejón, A. García, and J. M. Soler, Phys. Status Solidi B **215**, 809 (1999).

[31]A. S. Torralba, M. Todorovic, V. Brazdova, R. Choudhury, T. Miyazaki, M. J. Gillan, and D. R. Bowler, J. Phys. Condens. Matter **20**, 294206 (2008).

[32]M. Chen, G.-C. Guo, and L. He, J. Phys. Condens. Matter **22**, 445501 (2010).

[33]M. J. Louwerse and G. Rothenberg, Phys. Rev. B **85**, 035108 (2012).

[34]G. Lippert, J. Hutter, and M. Parrinello, Mol. Phys. **92**, 477 (1997).

[35]J. VandeVondele, M. Krack, F. Mohamed, M. Parrinello, T. Chassaing, and J. Hutter, Comput. Phys. Commun. **167**, 103 (2005).

[36]L. Fusti-Molnar and P. Pulay, J. Chem. Phys. **117**, 7827 (2002).

[37]M. A. Watson, Y. Kurashige, T. Nakajima, and K. Hirao, The Journal of Chemical Physics **128**, 054105 (2008).

[38]E. Hernández, M. J. Gillan, and C. M. Goringe, Phys. Rev. B **55**, 13485 (1997).

[39]N. Branda, R. Wyler, and J. Rebek, Science **263** (1994).

[40]S. Fox, H. G. Wallnoefer, T. Fox, C. S. Tautermann, and C.-K. Skylaris, J. Chem. Theory Comput. **7**, 1102 (2011).

[41]M. C. Payne, M. P. Teter, D. C. Allan, T. A. Arias, and J. D. Joannopoulos, Rev. Mod.

Phys. **64**, 1045 (1992).

[42]C.-K. Skylaris, A. A. Mostofi, P. D. Haynes, O. Diéguez, and M. C. Payne, Phys. Rev. B **66**, 035119 (2002).

[43]C.-K. Skylaris and P. D. Haynes, J. Chem. Phys. **127** (2007), 10.1063/1.2796168.

[44]C.-K. Skylaris, A. A. Mostofi, P. Haynes, C. J. Pickard, and M. C. Payne, Comput. Phys. Commun. **140**, 315 (2001).

[45]P. D. Haynes, C. K. Skylaris, A. A. Mostofi, and M. C. Payne, J. Phys.: Condens. Matter **20** (2008).

[46]X. P. Li, R. W. Nunes, and D. Vanderbilt, Phys. Rev. B **47**, 10891 (1993).

[47]N. D. M. Hine, M. Robinson, P. D. Haynes, C. K. Skylaris, M. C. Payne, and A. A. Mostofi, Phys. Rev. B **83**, 195102 (2011).

[48]C.-K. Skylaris, O. Diéguez, P. D. Haynes, and M. C. Payne, Phys. Rev. B **66**, 073103 (2002).

[49]T. Miyazaki, D. R. Bowler, R. Choudhury, and M. J. Gillan, J. Chem. Phys. **121**, 6186 (2004).

[50]E. Artacho, E. Anglada, O. Dièguez, J. D. Gale, A. García, J. Junquera, R. M. Martin, P. Ordejón, J. M. Pruneda, D. Sãnchez-Portal, and J. M. Soler, J. Phys. Condens. Matter **20**, 064208 (2008).

[51]M. Tafipolsky and R. Schmid, The Journal of Chemical Physics **124**, 174102 (2006).

[52]J. P. Perdew, K. Burke, and M. Ernzerhof, Phys. Rev. Lett. **77**, 3865 (1996).

[53]B. G. Pfrommer, M. Cote, S. G. Louie, and M. L. Cohen, J. Comput. Phys. **131**, 233 (1997).

[54]P. D. Haynes, C.-K. Skylaris, A. A. Mostofi, and M. C. Payne, Chemical Physics Letters **422**, 345 (2006).

[55]D. A. Case, T. A. Darden, I. T. E. Cheatham, C. L. Simmerling, J. Wang, R. E. Duke, R. Luo, R. C. Walker, W. Zhang, K. M. Merz, B. P. Roberts, B. Wang, S. Hayik, A. Roitberg, G. Seabra, I. Kolossváry, K. F. Wong, F. Paesani, J. Vanicek, J. Liu, X. Wu, S. R. Brozell, T. Steinbrecher, H. Gohlke, Q. Cai, X. Ye, J. Wang, M.-J. Hsieh, G. Cui, D. Roe, D. H. Mathews, M. Seetin, C. Sagui, V. Babin, T. Luchko, S. Gusarov, A. Kovalenko, and P. A. Kollman, "Amber 11," (2010).

[56]J. Harris, Phys. Rev. B **31**, 1770 (1985).

[57]W. M. C. Foulkes and R. Haydock, Phys. Rev. B **39**, 12520 (1989).